



Freezing of axisymmetric liquid bridges

Weiqi Huang ^{1,2} and Xinping Zhou ^{1,*}¹*School of Mechanical Science and Engineering, Huazhong University of Science and Technology, Wuhan 430074, People's Republic of China*²*Department of Mechanics, Huazhong University of Science and Technology, Wuhan 430074, People's Republic of China*

(Received 19 January 2020; accepted 16 September 2020; published 16 October 2020)

The solidification of liquid bridges plays an important role in many applications. Previous research on droplet solidification has found that supercooling and gravity have certain effects on physical properties and droplet shape during solidification. In this paper, axisymmetric water bridge solidification is studied from theory and experiment. A fixed contact line model, considering both the effects of supercooling and gravity, is developed to describe the freezing behavior of a liquid bridge. In the experiment, two horizontal cold coaxial circular end plates are cooled simultaneously, and a liquid bridge starts freezing from the contact surfaces with the end plates and finally forms an asymmetric ice ring in the middle. A correlation expression of the three-phase contact line height evolution determined by theory and experiment is developed. Comparisons between the calculation and experiment are made, and good agreement is obtained in the first freezing stage.

DOI: [10.1103/PhysRevFluids.5.103601](https://doi.org/10.1103/PhysRevFluids.5.103601)

I. INTRODUCTION

Liquid water solidification is a very common phenomenon in Nature and it is undesirable in many various industrial and environmental fields, such as power [1,2], aircraft [3,4], refrigeration [5,6], and meteorology [7]. The solidification of liquid water also has important applications in industry. In cryogenic grippers working in dry media [8,9], a water bridge is formed between the gripper and the target object, and the object is caught by freezing the liquid bridge. It is a very useful tool in the processes of microrobots, biology, optical, mechanical, and electrical micro- and even nanoscale manipulation and assembly. In container-free floating zone crystal growth [10,11], a feed rod melts in the floating zone and forms a liquid bridge. Then the molten zone solidifies from below by moving the floating zone and high purity crystals are produced. The densities of the melted feed rod, e.g., made from Si or GaSb, are greater than those of the respective solids. This technology is widely used in the preparation of semiconductor materials [12]. Surek *et al.* [13–15] claimed that the silicon crystal during growth can be shaped by meniscus control in the edge-defined film-fed growth technique. In fact, liquid freezing undergoes a crystallization process, and is accompanied by the release of latent heat, an increase in volume, and a significant change in physical properties, especially in the case of a large supercooling degree. Studying the evolution of the shape of a liquid bridge as it solidifies is not only helpful for a basic understanding of freezing phenomena, but also for improving industrial applications. Other industrial applications like coating technologies [16] and three-dimensional (3D) printing [17,18] may be improved from the studies of liquid bridge solidification.

*xpzhou08@hust.edu.cn

According to the temperature measurement results, the freezing process can be divided into four stages [19,20]: (1) liquid cooling (supercooling), (2) nucleation and recalescence, (3) freezing, and (4) solid cooling. Nucleation occurs at an arbitrary point on the solid substrate in the form of heterogeneous nucleation, followed by rapid kinetic crystal growth in the recalescence stage [21]. During this period, supercooling drives the growth of microscopic dendritic ice structures, which eventually fill the entire volume of the liquid. At the end of the nucleation-recalescence stage, the liquid becomes a homogeneous mushy zone consisting of ice and water, which can be visualized as a sudden change in liquid opacity in experiments [21–24].

Previous research focused on the freezing process of water droplets [21,23] and, to date, there have been only a few studies about liquid bridge freezing. Martínez *et al.* [25] conducted a solidification experiment of a liquid bridge with fixed contact lines under microgravity on a TEXUS-18 sounding-rocket flight. Cröll *et al.* [12] used the floating zone method to prepare crystals under microgravity, and found that the noncrystalline molten feed rod formed a nonaxisymmetric ring-shaped protruding structure after solidification. To determine the cohesion and adhesion of the ice bridge, Lehnert-Batar [26] froze a liquid bridge from the top under the effect of gravity. A ring along the circumference at the lower part of the ice bridge or an excrescence was observed. The liquid bridge was formed between two horizontal plates with nonfixed contact lines and the radius of the lower contact line is larger than the upper one due to gravity. In the previous studies, liquid bridges solidified from a single contact surface, and they rarely reflected the significance of supercooling to the solidification process while some of them ignored the effect of gravity. Gravity may alter the liquid bridge shape while the supercooling can change mushy zone properties such as the thermal capacity, thermal conductivity, and latent heat. These parameters will greatly affect the solidification rate and time [27].

In this paper, the freezing processes of a liquid bridge between equal cold coaxial end plates are studied experimentally. The liquid bridge starts solidifying from two circular end plates. The freezing behaviors are characterized by the triple-phase contact line, and the profile and volume of the liquid bridge. In addition, a theoretical model is developed to describe the evolution of the liquid bridge profile during the freezing process based on previous work [27–30]. The effect of supercooling on physical properties and the effects of gravity and volume expansion on the shape of the liquid bridge are taken into account in this model. The mass fraction of ice at the end of the nucleation-recalescence stage is calculated from the supercooling degree, which can further determine the physical properties of the mushy zone [19,20,27,31]. The model contains the evolution correlation of the triple-phase contact line height which is determined based on the experimental data.

II. EXPERIMENTAL SETUP AND METHOD

A schematic diagram of the experimental setup is shown in Fig. 1. The apparatus consists of four parts: testing section, semiconductor thermoelectric cooling system, data collection system, and image acquisition system.

The cooling system and testing section constitute two symmetrical parts including the upper and lower parts. Each part is composed of a cooling bath, a semiconductor cooler, two square copper sheets, and a circular copper sheet. Cool water in the cooling bath can take away the heat generated by the semiconductor cooler (TEC1-01705), which is used to cool down the end plate based on the Peltier effect. The semiconductor cooler is connected to a programmable dc power supply, which is controlled by EASYHOST 6.2 software (Oeshine, China). The size of each square copper sheet is 15 mm × 15 mm × 1 mm. The circular copper sheet is 1 mm in thickness, which is used as the end plate for fixing the initial contact line of the liquid bridge. All the above components are connected with thermal grease to reduce the contact thermal resistance. The distance between the upper and lower parts can be adjusted.

The data acquisition unit (Omega DAQ-3005, USA) and the thermocouple (0.1 mm in diameter, calibrated by a standard thermometer) buried between the two adjacent square copper sheets consti-

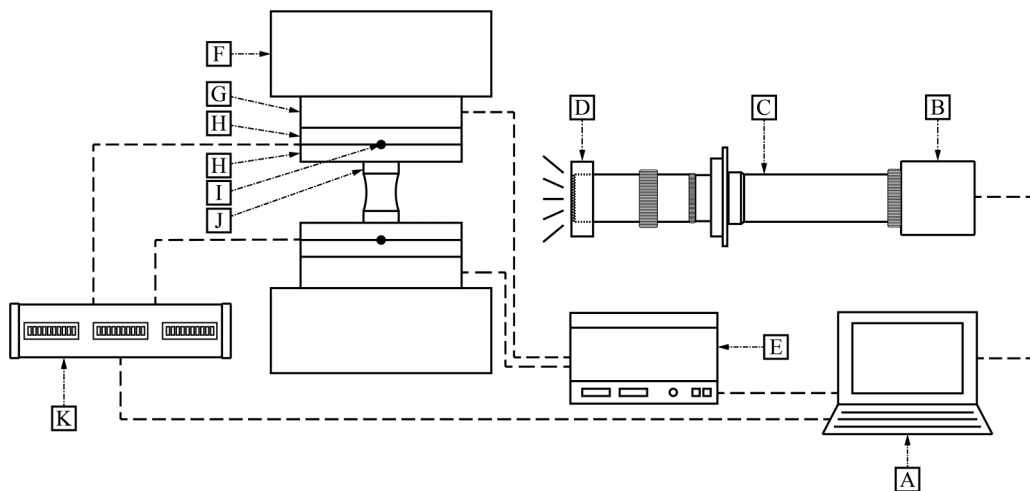


FIG. 1. Schematic of experimental system: (A) computer, (B) CCD camera, (C) long distance microscope, (D) ring cold light, (E) power supply, (F) cooling bath, (G) semiconductor cooler, (H) copper plate, (I) thermocouple, (J) copper end plate, and (K) temperature acquisition unit.

tute the data acquisition system. Because of the high thermal conductivity of copper (399 W/mK), the temperature measured by the thermocouple can be regarded as the end plate temperature.

The image acquisition system includes a charge-coupled device (CCD) camera (Edmund 2323c, USA), a long distance microscope (Edmund VZM450i, USA), and a diffused cold light source. The freezing behaviors of the liquid bridge are recorded by the camera from the side of the disks at a rate of 60 frames per second with a resolution of $1920 \text{ pixels} \times 1200 \text{ pixels}$.

The experiment is conducted at atmospheric pressure and at an ambient temperature of $20.0 \text{ }^\circ\text{C} \pm 0.5 \text{ }^\circ\text{C}$ and relative humidity of $40\% \pm 1\%$. In the experiment, water drops are generated by the microsyringe and placed on an end plate; then the other end plate is moved to contact the water drop and form a liquid water bridge which is pinned on the edge of the end plate. Next, we adjust the height of the liquid bridge to meet the experimental requirement. Finally, we make it cool down and freeze. The temperature of the cold end plates maintains at $0.5 \text{ }^\circ\text{C}$ during the formation of a desired liquid bridge to minimize its evaporation. In order to ensure that the temperature of the supercooling liquid bridge is uniform and the temperatures of the end plates are basically unchanged during the freezing stage, the cooling rate of the end plates is controlled to be $1 \text{ }^\circ\text{C}/\text{min}$. Therefore, the liquid bridge temperature during nucleation (T_N) can be regarded as the end plate temperature (T_C), as noted in Fig. 2.

III. THEORETICAL MODEL

A. Initial liquid bridge shape

A liquid can be held between two horizontal circular end plates to form a liquid bridge (see Fig. 2). The liquid bridge's contact lines are pinned on the edges of end plates by surface tension, γ . The influence of gravity on the liquid bridge's shape is characterized by the Bond number, $B = \rho g R_p^2 / \gamma$ where R_p is the radius of the end plate, g is the gravitational acceleration, and ρ is the density difference between the liquid bridge and the ambient air. The gravity effect can be ignored when $B \ll 1$. In this experiment, the Bond number is computed to be about 0.14, meaning that the gravity cannot be negligible.

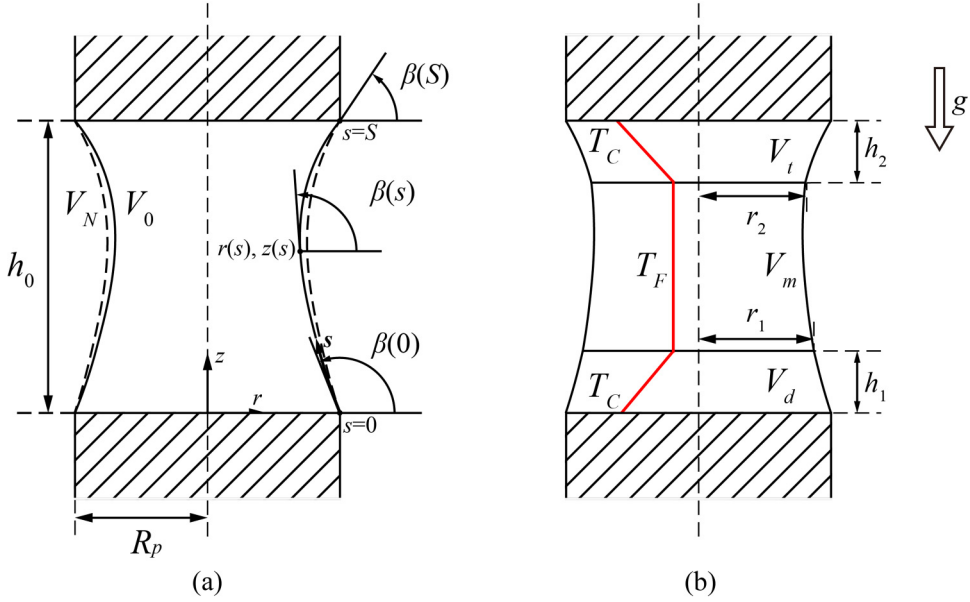


FIG. 2. Schematic of liquid bridge between equal end plates: (a) nucleation-recalescence; (b) freezing stage. T_F is the mushy zone temperature, and T_C is the end plate temperature, which can be regarded as the nucleation temperature T_N .

The Young-Laplace equation of the axisymmetric liquid bridge can be expressed according to the arc length in the r - z plane [32–34]. The Young-Laplace equation of the fixed contact line can be described by a second-order system,

$$\begin{aligned} r'' &= -\beta' z' \\ z' &= \beta' r' \\ \beta' &= Q - Bz - z'/r, \end{aligned} \quad (3.1)$$

with the initial and boundary conditions

$$\begin{aligned} r(0) &= r(S) = R_p, \\ z(0) &= 0, \quad z(S) = H, \\ \int_0^H \pi r^2 dz &= V_0, \end{aligned} \quad (3.2)$$

where the superscript indicates the derivative of arc length $\partial/\partial s$, S is the total arc length, H is the distance between two end plates, V_0 is the volume of the liquid bridge, $\beta(s)$ is the angle between the r axis and the tangent to the equilibrium profile, and Q is an unknown parameter characterized by the pressure jump between the liquid and the ambient air, which can be determined by the shooting method. The arc-length-based Young-Laplace equation allows simple calculation of equilibrium shapes of axisymmetric liquid bridges.

B. Nucleation-recalescence stage

A liquid bridge with a volume of V_0 , an end plate radius of R_p , and a height of H is slowly cooled down by the end plates. When the temperature of the bridge reaches the nucleation temperature of T_N , nucleation and recalescence will take place, and water instantly transforms into the mushy zone.

Its physical properties are different from water. The volume of the liquid bridge increases to V_N . The shape and contact angle of the liquid bridge will also change, which can be determined by (3.1) and (3.2) with changed volume. During the freezing stage, the liquid-solid front will advance until the mushy zone is completely solidified due to the continuous cooling of the cold. The problem can be simplified based on the assumptions as follows: (1) the shape remains axisymmetric, (2) the freezing fronts are planes parallel to the end plates, (3) the heat transfer in the ice layer is one-dimensional in the quasisteady state, and (4) the evaporation is weak and can be ignored. Schultz *et al.* [35] found that the interface stays fairly flat for much of the freezing process, and a nonplanar interface model may be important to capture more of the details near the final stage of freezing for a sessile water droplet. Related research [27] showed that the planar interface model can also predict the freezing shape of a sessile water droplet well before the final stage of freezing. In this paper, the theoretical model considering the planar solid-liquid interfaces only describes the freezing stage of the liquid bridge before the final stage of freezing, and does not involve the final freezing stage.

During the nucleation-recalescence stage, the volume and physical properties of the liquid bridge can change dramatically, which may severely affect the subsequent freezing stage. The volume and other properties after the nucleation-recalescence stage are determined by the mass fraction of ice. The mass fraction of ice can be calculated as [27,36]

$$f_i = \frac{c_{w,T_F}(T_F - T_N)}{L} = \frac{c_{w,T_F}}{c_i} \text{St}, \quad (3.3)$$

where T_F is the freezing temperature, which is equal to 0° for water; c_{w,T_F} is the water specific heat capacity at the freezing temperature; and L is the specific solidification latent heat of liquid water. Hence the temperature difference $T_F - T_N$ indicates the supercooling degree, which can be represented by ΔT . The Stefan number, $\text{St} = c_i(T_F - T_N)/L$, denotes the ratio of the sensible to latent heat.

With the ice mass fraction, the specific solidification latent heat (L_m) and density (ρ_m) of the mushy zone can be calculated from

$$L_m = (1 - f_i)L, \quad (3.4)$$

$$\rho_m = \rho_w(1 - f_i) + f_i\rho_i, \quad (3.5)$$

where ρ_i and ρ_w represent the densities of ice and water, respectively. The volume of the liquid bridge (V_N) when the nucleation-recalescence stage is completed can be obtained from

$$\rho_m V_N = \rho_w V_o. \quad (3.6)$$

C. Freezing stage

In the model of liquid drop freezing [27,28], the correlation used to describe the evolution of triple-phase contact line height can be written as

$$h(t) = \sqrt{XMt}, \quad (3.7)$$

where $M = k_i \Delta T / (\rho_i L_m)$ with k_i being the thermal conductivity of ice, and X is a correction coefficient which can be determined by experimental data.

We assume that when the freezing fronts are advancing, the contact line of the liquid bridge is fixed on the frozen ice layer due to surface tension. In the meanwhile, when the lower and upper freezing fronts are moving towards each other, the initial and boundary conditions of (3.1) will change. As the solidification process progresses, the shape of the liquid bridge constantly changes and further affects the subsequent solidification behavior.

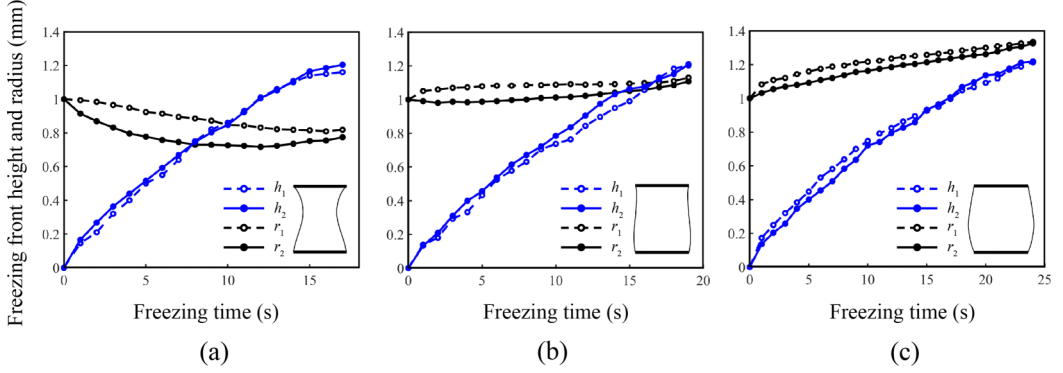


FIG. 3. Evolution of heights and radii of upper and lower freezing fronts of liquid bridges with different shapes: (a) slender ($R_p = 1$ mm, $H = 2.5$ mm, $V_0 = 5 \mu\text{l}$), (b) undulation ($R_p = 1$ mm, $H = 2.5$ mm, $V_0 = 7.5 \mu\text{l}$), and (c) rotund ($R_p = 1$ mm, $H = 2.5$ mm, $V_0 = 10 \mu\text{l}$), during the freezing process. The insets represent the shapes of the liquid bridges before freezing.

Since the freezing fronts are treated as planar surfaces, the mass conservation equation can be written as

$$\rho_m \frac{dV_{m,n}}{dt} = -\pi \rho_i r_n^2 \frac{dh}{dt}, \quad (3.8)$$

where V_m is the volume of the mushy zone. The subscripts $n = 1, 2$ denote the lower and upper ice layers, respectively. Because the temperatures of the upper and lower end plates are equal, (3.7) shows that $h_1 = h_2$ at the same time. This also can be proved by Fig. 3, which shows the evolution of the heights and radii of the freezing fronts for the liquid bridges of different shapes during the freezing process. It can be seen that due to the effect of gravity, the radius of the upper freezing front can become obviously smaller than that of the lower freezing front in some cases [e.g., the case as shown in Fig. 3(a)], but regardless of the shape of the liquid bridge, the height of the upper freezing front is basically equal to that of the lower freezing front. That is, $h = h_1 = h_2$. The volumes of upper and lower ice layers are, respectively,

$$\begin{aligned} V_i &= \int_h^H \pi r^2 dz, \\ V_d &= \int_0^h \pi r^2 dz. \end{aligned} \quad (3.9)$$

From (3.8) and (3.9), V_m can be determined. The shape of the mushy zone can be determined with V_m and the updated parameters (i.e., the height of the mushy zone, $H - 2h$, and the radius of the lower and upper ice layers, r_1 and r_2). It is worth noting that the mushy zone is fixed between unequal circular ice layers. The characteristic length of the Bond number should be replaced by the average radius which is $r_0 = (r_1 + r_2)/2$ [37].

The shape of the liquid bridge can be determined by (3.1) with the following updated initial and boundary conditions:

$$\begin{aligned} r(0) &= r_1, \quad r(S) = r_2, \\ z(0) &= 0, \quad z(S) = H - 2h, \\ \int_0^{H-2h} \pi r^2 dz &= V_m. \end{aligned} \quad (3.10)$$

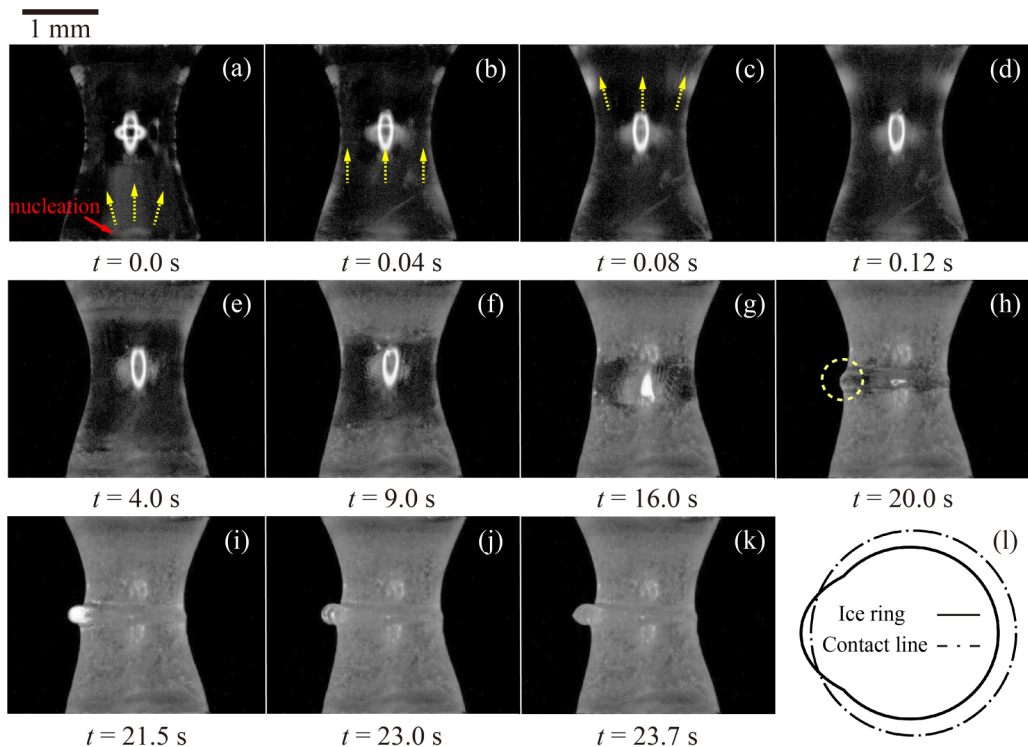


FIG. 4. Freezing process of a liquid bridge ($R_p = 1$ mm, $H = 2.75$ mm, $V_0 = 5.5 \mu\text{l}$). (a)–(d) Nucleation-recalescence stage; (d)–(k) freezing stage; (l) sketch of ice ring. Red arrow points out the nucleation position and yellow arrows indicate the direction of recalescence, while yellow circle in (h) indicates the single azimuthal bulge.

The variations of triple-phase contact line height and radius with time can be obtained by solving (3.1), (3.7), and (3.8)–(3.10). This model is only applicable to the first freezing stage of the liquid bridge. Freezing details are described in Sec. IV.

IV. RESULTS

A. Phenomenon observation

Figure 4 illustrates the freezing process of a $5.5\text{-}\mu\text{l}$ liquid bridge for $R_p = 1$ mm and $H = 2.75$ mm at an end plate temperature of $T_N = -10^\circ\text{C}$. As mentioned previously, the freezing process includes the nucleation-recalescence stage and the freezing stage. Figures 4(a)–4(d) correspond to the nucleation-recalescence stage, and Figs. 4(d)–4(k) correspond to the freezing stage.

In the nucleation-recalescence stage, the liquid bridge turns into a homogeneous mixed-phase state and changes from transparent [see Fig. 4(a)] to translucent [see Fig. 4(d)] [38]. As shown in Fig. 4(a), nucleation starts from the bottom end plate (marked by the red arrow) and crystal growth rapidly spreads across the entire liquid bridge within 120 ms (marked by yellow arrows). Freezing will start once the nucleation-recalescence process is completed.

In the freezing stage, the freezing fronts move between the top and bottom end plates as solidification progresses, and the movement slows down gradually because the thickened ice layers increase the thermal resistance. According to whether the liquid bridge is stable or unstable, the freezing can be divided into two stages. In the first freezing stage, corresponding to Figs. 4(d)–4(g), the liquid bridge continuously expands radially under the compression of the upper and lower ice layers, and the liquid bridge is in a stable state. In the second stage of freezing corresponding to Figs. 4(h)–4(k),

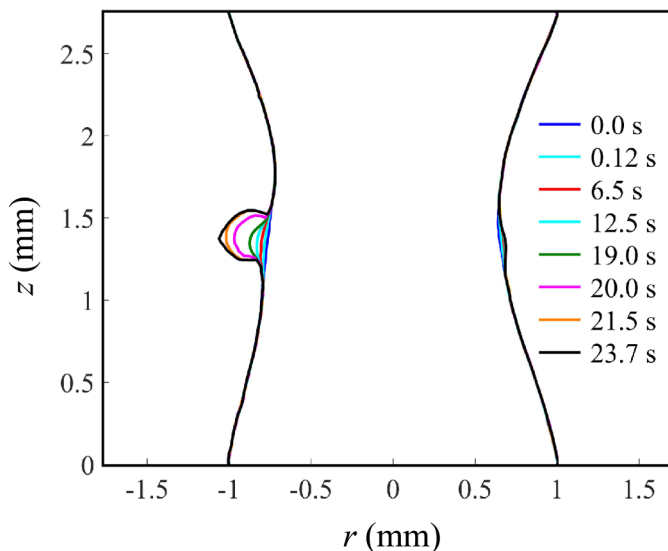


FIG. 5. Evolution of liquid bridge profile during freezing process ($R_p = 1$ mm, $H = 2.75$ mm, $V_0 = 5.5 \mu\text{l}$).

the liquid bridge produces a single azimuthal bulge, which forms a nonaxisymmetric ice ring in the center of the liquid bridge at the end of the freezing stage. The liquid bridge forms an azimuthal bulge at 20 s, which is marked by a yellow circle. From the side view shown in Fig. 4(k), the protruding part of the ice ring has a freezing shape similar to a liquid drop which is solidified on a vertical cold wall [39]. Figure 4(l) gives a top view of the ice ring. It is worth noting that the protruding location of the ice ring is the position where the azimuthal bulge forms.

The liquid bridge will expand radially during the freezing process. As depicted in Fig. 5, corresponding to Fig. 4, it demonstrates the evolution of the liquid bridge profile obtained from experiment using image recognition technology. Table I gives the physical properties of liquid water and ice at the temperature of 0°C . Based on these parameters, the initial ice mass fraction after the nucleation-recalescence stage can be calculated by (3.3) to be 8.26%, which corresponds to a liquid bridge with an initial volume of $5.5 \mu\text{l}$ and a nucleation-recalescence volume of $5.56 \mu\text{l}$. It agrees well with the corresponding volumes of 5.5 and $5.55 \mu\text{l}$ obtained from Fig. 5.

The evolution and expansion rate of the droplet volume can be calculated and the results are shown in Fig. 6. The volume expands sharply in the nucleation-recalescence stage. As the freezing process goes on, the water turns into ice and the liquid bridge volume increases. Because of the growth of the ice layers' thickness, the thermal resistance increases and the volume expansion rate decreases. The final liquid bridge volume is $5.95 \mu\text{l}$ and the resulting expansion ratio is 1.082. This good agreement between theory and experiment also provides reliability for experimental data.

TABLE I. Physical properties of ice at different temperatures and liquid water [41].

Material	Temperature ($^\circ\text{C}$)	Density (kg/m^3)	Specific heat capacity ($\text{kJ}/\text{kg K}$)	Thermal conductivity (W/mK)	Specific latent heat (kJ/kg)
Liquid water		999.8	4.22	0.56	333.4
Ice	0	916.7	2.10	2.16	
Ice	-3.65	917.3	2.07	2.19	
Ice	-5	917.4	2.06	2.21	

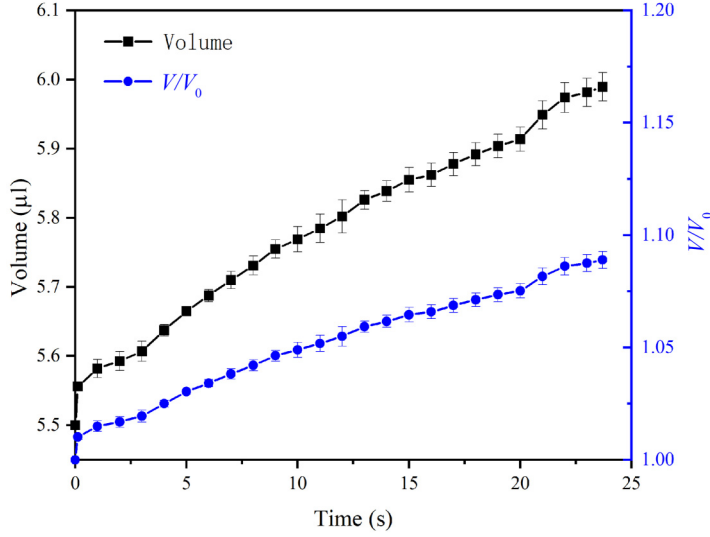


FIG. 6. Evolution of liquid bridge volume and expansion rate during freezing process ($R_p = 1$ mm, $H = 2.75$ mm, $V_0 = 5.5$ μl).

B. Determination of correlation

Figure 7(a) shows the evolution of the triple-phase contact line average height (h) at different nucleation temperatures (T_N) and liquid bridge volumes (V_0) after nucleation-recalescence is completed. Figure 7(b) shows the variation of h with the combined variable of \sqrt{Mt} (unit: mm), which

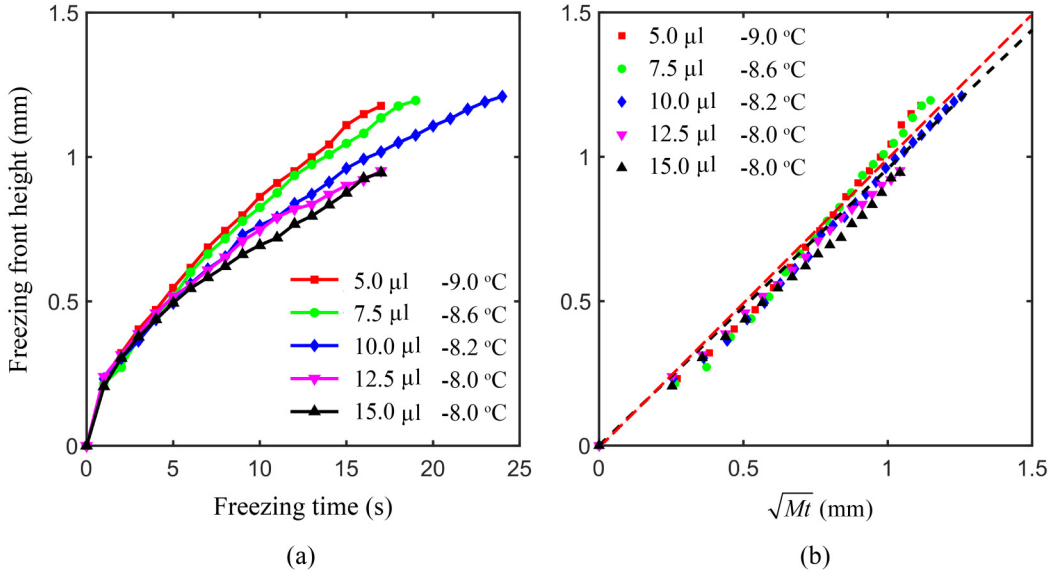


FIG. 7. Evolution of freezing front average heights at different liquid bridge volumes and nucleation temperatures during the first freezing stage ($R_p = 1$ mm, $H = 2.5$ mm): (a) experimental data; (b) normalized results and fitting results. The black and red dotted fitting lines in (b) are $X = 0.92$ ($R^2 = 0.9932$) and 1 ($R^2 = 0.9911$), respectively.

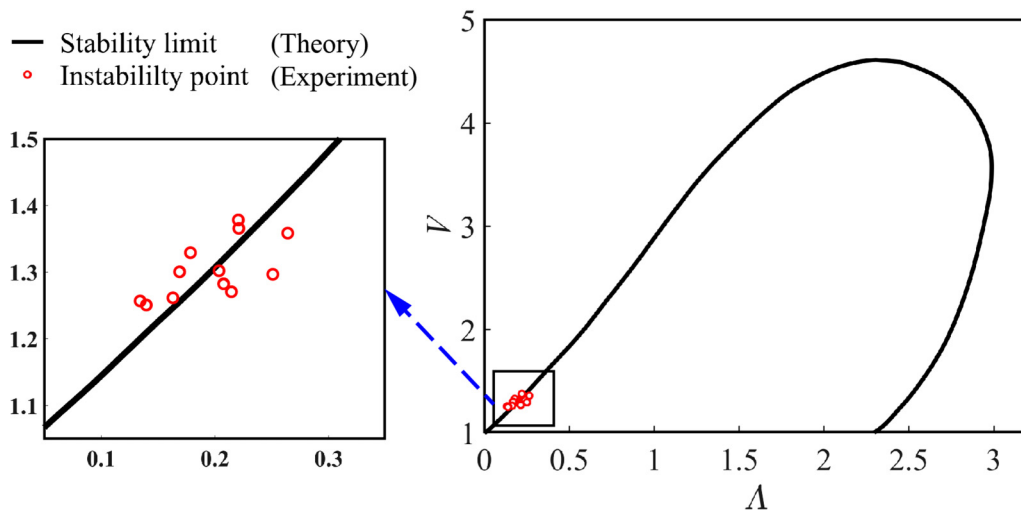


FIG. 8. The parameters of liquid bridges when the single azimuthal bulge is about to form are depicted on the stability diagram of a liquid bridge. The experimental points are basically distributed on the stability limit of the liquid bridge, so it can be judged that the liquid bridges are unstable.

has been selected according to (3.7). The model is only applicable to the liquid bridge in the stable state. Accordingly, Fig. 7 only shows the height data in the first freezing stage. It can be seen from Fig. 7(a) that different conditions will lead to different growth rates of h . The data points of Fig. 7(b) are distributed along the fitting straight lines [plotted as black dotted lines in Fig. 7(b)], and the correction coefficient in (3.7) for the liquid bridge freezing in the first freezing stage is determined based on the experimental data.

Figure 8 plots the points representing the critical parameters of the liquid bridge at the time when a single azimuthal bulge is generated, and the curve of the stability limit of the liquid bridge with $B = 0.14$ is shown [32,33,37]. The horizontal and vertical coordinates denote the aspect ratio [$\Lambda = (H - 2h)/(r_1 + r_2)$] and the dimensionless volume ($V = 4V_m/[\pi(r_1 + r_2)^2(H - 2h)]$), respectively. It can be seen that the points representing the critical parameters of the liquid bridge at the time when the bulge is formed are basically distributed on the stability limit curve. The theoretical results about the stability limit are in good agreement with the experimental measurements regarding the formation of the bulge. It can be inferred that the formation of the bulge is caused by the instability of the liquid bridge, which has been reported by Russo *et al.* [40].

C. Comparison between experiment and model

Since the correlation for the evolution of h has been determined by (4.1), the evolution of the liquid bridge shape in the first stage of freezing can be simulated. A liquid bridge with a volume of $V_0 = 5.5 \mu\text{l}$ and a height of $H = 2 \text{ mm}$ is chosen for calculation, and relevant parameters of water and ice are presented in Table I. The ice mass fraction f_i is 0.092 and the specific latent heat L_m is 302.6 kJ/kg, both of which are computed for $T_N = -7.3 \text{ }^\circ\text{C}$. The average temperature of the ice layers is calculated by $(T_F + T_N)/2$, where T_F and T_N are the top and bottom surface temperatures, respectively. In this model, the thermophysical properties of ice at $-3.65 \text{ }^\circ\text{C}$ are used. Figure 9 compares the liquid bridge shapes at different times obtained from the model and the experiment. The shape at the beginning of the nucleation-recalescence stage and that at the end of such a stage correspond to $t = 0.0 \text{ s}$ and $t = 0.15 \text{ s}$, respectively. The shape at $t = 15.0 \text{ s}$ is the final shape in the first freezing stage. The shape at $t = 0.15 \text{ s}$ is slightly more expanded than that at $t = 0.0 \text{ s}$, because

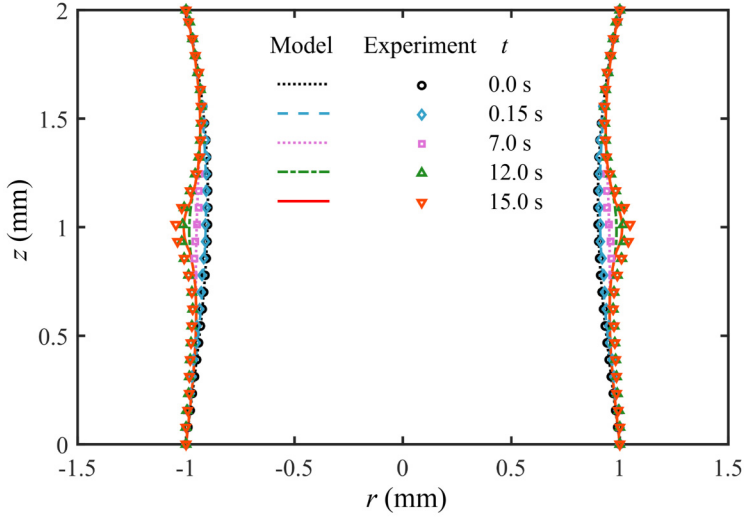


FIG. 9. Evolution of liquid bridge profiles obtained from calculation and experiment ($R_p = 1$ mm, $H = 2$ mm, $V_0 = 5.5 \mu\text{l}$).

little water changes into ice. Due to the constraint in the longitudinal direction, the expansion of the liquid bridge can only occur in the radial direction, reflected by the increase of the radius. As time goes by, more water turns into ice, and the radial expansion of the liquid bridge increases.

Figure 10 compares the triple-phase contact line heights and radii of the liquid bridge at different times between the calculated results and the experimental data. The height increases with time, and the freezing rate decreases due to the increase of the thermal resistance caused by the ice layers thickening. Good agreement in height is observed, while the experimental value of the radius is getting larger than that of the model. This deviation is within 7.4% at the end of the first freezing stage. We speculate that this deviation is attributed to the planar freezing front assumption while the freezing front is a curved surface in the freezing process of the droplet [23,24].

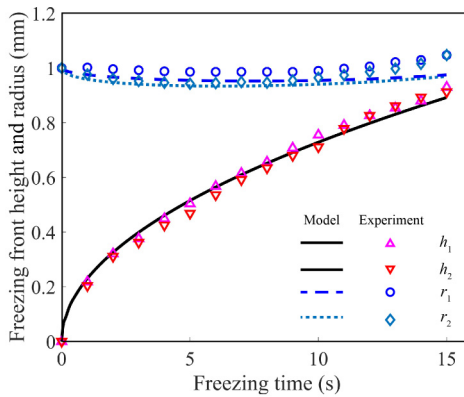


FIG. 10. Comparison between calculation and experiment of the evolution of triple-phase contact line height and radius ($R_p = 1$ mm, $H = 2$ mm, $V_0 = 5.5 \mu\text{l}$).

V. CONCLUSIONS

In this paper, the experiment of solidification of a liquid bridge has been conducted under different experimental conditions. The evolution of the profile and volume of the liquid bridge has been obtained. We have proposed a model to describe freezing behaviors. The following conclusions are drawn.

(1) The freezing of the liquid bridge can be divided into two stages according to the stability of the liquid bridge. The liquid bridge eventually becomes unstable and freezes to form an ice ring.

(2) The volume of the liquid bridge increases sharply in the nucleation-recalescence stage. As time goes on, the volume expansion rate decreases due to the increase in thermal resistance caused by the thickening of the ice layers.

(3) The model describes the evolution of freezing the liquid bridge in the first freezing stage by assuming a planar freezing front.

In the present investigation, due to limitations in the experimental range, the freezing phenomenon of a liquid bridge, especially the formation of an ice ring, could not be studied systematically. Besides, because of the randomness of the location where the bulge occurs, the protruding of the ice ring may occur on any side of the liquid bridge, and it is difficult to observe it systematically. For further research, a two-camera orthogonal observation experiment and numerical simulation are necessary.

ACKNOWLEDGMENT

This research was supported in part by the National Natural Science Foundation of China (Grant No. 11972170).

-
- [1] L. Gao, Y. Liu, and H. Hu, An experimental investigation on the dynamic glaze ice accretion process over a wind turbine airfoil surface, *Int. J. Heat Mass Transfer* **149**, 119120 (2020).
 - [2] J. Laforte, M. Allaire, and J. Laflamme, State-of-the-art on power line de-icing, *Atmos. Res.* **46**, 143 (1998).
 - [3] Z. A. Janjua, B. Turnbull, S. Hibberd, and K.-S. Choi, Mixed ice accretion on aircraft wings, *Phys. Fluids* **30**, 027101 (2018).
 - [4] Y. Cao, Z. Wu, Y. Su, and Z. Xu, Aircraft flight characteristics in icing conditions, *Prog. Aeronaut. Sci.* **74**, 62 (2015).
 - [5] D. L. da Silva, C. Melo, and C. J. L. Hermes, Effect of frost morphology on the thermal-hydraulic performance of fan-supplied tube-fin evaporators, *Appl. Therm. Eng.* **111**, 1060 (2017).
 - [6] M. A. Rahman and A. M. Jacobi, Experimental study on frosting/defrosting characteristics of microgrooved metal surfaces, *Int. J. Refrig.* **50**, 44 (2015).
 - [7] H. J. Punge and M. Kunz, Hail observations and hailstorm characteristics in Europe: A review, *Atmos. Res.* **176–177**, 159 (2016).
 - [8] D. Lang, I. Kurniawan, M. Tichem, and B. Karpuschewski, First investigations on force mechanisms in liquid solidification micro-gripping, in *Proceedings of the 6th IEEE International Symposium on Assembly and Task Planning: From Nano to Macro Assembly and Manufacturing* (IEEE, Piscataway, NJ, 2005).
 - [9] B. López-Walle, M. Gauthier, and N. Chaillet, Principle of a submerged freeze gripper for microassembly, *IEEE Trans. Rob.* **24**, 897 (2008).
 - [10] Q. Ren, H. Su, J. Zhang, W. Ma, Y. Cao, J. Chen, L. Liu, and H. Fu, Directional solidification and growth characteristics of $\text{Al}_2\text{O}_3/\text{Er}_3\text{Al}_5\text{O}_{12}/\text{ZrO}_2$ ternary eutectic ceramic by laser floating zone melting, *J. Mater. Sci.* **52**, 5559 (2017).
 - [11] I. Martinez and A. Eyer, Liquid bridge analysis of silicon crystal growth experiments under microgravity, *J. Cryst. Growth* **75**, 535 (1986).

- [12] A. Cröll, T. Kaiser, M. Schweizer, A. Danilewsky, S. Lauer, A. Tegetmeier, and K. Benz, Floating-zone and floating-solution-zone growth of GaSb under microgravity, *J. Cryst. Growth* **191**, 365 (1998).
- [13] T. Surek and B. Chalmers, The direction of growth of the surface of a crystal in contact with its melt, *J. Cryst. Growth* **29**, 1 (1975).
- [14] T. Surek, B. Chalmers, and A. I. Mlavsky, The edge-defined film-fed growth of controlled shape crystals, *J. Cryst. Growth* **42**, 453 (1977).
- [15] L. Eriss, R. W. Stormont, T. Surek, and A. S. Taylor, The growth of silicon tubes by the EFG process, *J. Cryst. Growth* **50**, 200 (1980).
- [16] A. G. González, J. A. Diez, R. Gratton, D. M. Campana, and F. A. Saita, Instability of a viscous liquid coating a cylindrical fibre, *J. Fluid Mech.* **651**, 117 (2010).
- [17] W. Feng, Y. Chai, J. Forth, P. D. Ashby, T. P. Russell, and B. A. Helms, Harnessing liquid-in-liquid printing and micropatterned substrates to fabricate 3-dimensional all-liquid fluidic devices, *Nat. Commun.* **10**, 1095 (2019).
- [18] M. Cavaiani, S. Dehaeck, Y. Vitry, and P. Lambert, Multi-scale 3D printed capillary gripper, in *Proceedings of the 2018 International Conference on Manipulation, Automation and Robotics and Small Scales* (IEEE, Piscataway, NJ, 2018).
- [19] J. P. Hindmarsh, A. B. Russell, and X. D. Chen, Experimental and numerical analysis of the temperature transition of a freezing food solution droplet, *Chem. Eng. Sci.* **59**, 2503 (2004).
- [20] J. P. Hindmarsh, A. B. Russell, and X. D. Chen, Experimental and numerical analysis of the temperature transition of a suspended freezing water droplet, *Int. J. Heat Mass Transfer* **46**, 1199 (2003).
- [21] M. Schremb and C. Tropea, Solidification of supercooled water in the vicinity of a solid wall, *Phys. Rev. E* **94**, 052804 (2016).
- [22] X. Zhang, X. Wu, and J. Min, Freezing and melting of a sessile water droplet on a horizontal cold plate, *Exp. Therm. Fluid Sci.* **88**, 1 (2017).
- [23] A. G. Marin, O. R. Enriquez, P. Brunet, P. Colinet, and J. H. Snoeijer, Universality of Tip Singularity Formation in Freezing Water Drops, *Phys. Rev. Lett.* **113**, 054301 (2014).
- [24] O. R. Enríquez, Á. G. Marín, K. G. Winkels, and J. H. Snoeijer, Freezing singularities in water drops, *Phys. Fluids* **24**, 091102 (2012).
- [25] I. Martínez, A. Sanz, J. M. Perales, and J. Meseguer, Freezing of a long liquid column on the Texas-18 sounding rocket flight, *ESA J.* **12**, 483 (1988).
- [26] S. Lehnert-Batar, Freezing of axisymmetric water bridges between two horizontal surfaces, Ph.D. thesis, Swiss Federal Institute of Technology Zurich, 1999.
- [27] X. Zhang, X. Wu, J. Min, and X. Liu, Modelling of sessile water droplet shape evolution during freezing with consideration of supercooling effect, *Appl. Therm. Eng.* **125**, 644 (2017).
- [28] X. Zhang, X. Liu, J. Min, and X. Wu, Shape variation and unique tip formation of a sessile water droplet during freezing, *Appl. Therm. Eng.* **147**, 927 (2019).
- [29] M. Nauenberg, Theory and experiments on the ice-water front propagation in droplets freezing on a subzero surface, *Eur. J. Phys.* **37**, 045102 (2016).
- [30] J. H. Snoeijer and P. Brunet, Pointy ice-drops: How water freezes into a singular shape, *Am. J. Phys.* **80**, 764 (2012).
- [31] T. Sorgenfrei, 30 years of crystal growth under microgravity conditions in Freiburg: An overview of past activities, *Cryst. Res. Technol.* **53**, 1700265 (2018).
- [32] B. J. Lowry and P. H. Steen, Capillary surfaces: Stability from families of equilibria with application to the liquid bridge, *Proc. R. Soc. London, Ser. A* **449**, 411 (1995).
- [33] L. A. Slobozhanin and J. M. Perales, Stability of liquid bridges between equal disks in an axial gravity field, *Phys. Fluids A* **5**, 1305 (1993).
- [34] A. D. Myshkis, V. G. Babskii, N. D. Kopachevskii, L. A. Slobozhanin, A. D. Tyuptsov, and R. Wadhwa, *Low-Gravity Fluid Mechanics* (Springer, New York, 1987).
- [35] W. W. Schultz, M. G. Worster, and D. M. Anderson, Solidifying sessile water droplets, in *Interactive Dynamics of Convection and Solidification*, edited by P. Ehrhard, D. S. Riley, and P. H. Steen (Springer, Dordrecht, 2001), pp. 209–226.

- [36] X. Zhang, X. Liu, X. Wu, and J. Min, Simulation and experiment on supercooled sessile water droplet freezing with special attention to supercooling and volume expansion effects, *Int. J. Heat Mass Transfer* **127**, 975 (2018).
- [37] L. A. Slobozhanin and J. I. D. Alexander, Combined effect of disk inequality and axial gravity on axisymmetric liquid bridge stability, *Phys. Fluids* **10**, 2473 (1998).
- [38] S. Jung, M. K. Tiwari, N. V. Doan, and D. Poulikakos, Mechanism of supercooled droplet freezing on surfaces, *Nat. Commun.* **3**, 615 (2012).
- [39] V. N. Duy and T. V. Vu, A numerical study of a liquid drop solidifying on a vertical cold wall, *Int. J. Heat Mass Transfer* **127**, 302 (2018).
- [40] M. J. Russo and P. H. Steen, Instability of rotund capillary bridges to general disturbances: Experiment and theory, *J. Colloid Interface Sci.* **113**, 154 (1986).
- [41] W. M. Haynes, *CRC Handbook of Chemistry and Physics* (CRC Press, Boca Raton, FL, 2014).